Ongoing transients in carbonate compensation

Bernard P. Boudreau,[1] Jack J. Middelburg,[2,3] Andreas F. Hofmann,[3,4] and Filip J. R. Meysman[3,5]

Received 15 August 2009; revised 29 June 2010; accepted 13 July 2010; published 4 November 2010.

[1] Uptake of anthropogenic CO_2 is acidifying the oceans. Over the next 2000 years, this will modify the dissolution and preservation of sedimentary carbonate. By coupling new formulas for the positions of the calcite saturation horizon, z_{sat}, the compensation depth, z_{cc}, and the snowline, z_{snow}, to a biogeochemical model of the oceanic carbonate system, we evaluate how these horizons will change with ongoing ocean acidification. Our model is an extended Havardton-Bear-type box model, which includes novel kinetic descriptions for carbonate dissolution above, between, and below these critical depths. In the preindustrial ocean, z_{sat} and z_{cc} are at 3939 and 4750 m, respectively. When forced with the IS92a CO_2 emission scenario, the model forecasts (1) that z_{sat} will rise rapidly ("runaway" conditions) so that all deep water becomes undersaturated, (2) that z_{cc} will also rise and over 1000 years will pass before it will be stabilized by the dissolution of previously deposited $CaCO_3$, and (3) that z_{snow} will respond slowly to acidification, rising by ~1150 m during a 2000 year timeframe. A further simplified model that equates the compensation and saturation depths produces quantitatively different results. Finally, additional feedbacks due to acidification on calcification and increased atmospheric CO_2 on organic matter productivity strongly affect the positions of the compensation horizons and their dynamics.

Citation: Boudreau, B. P., J. J. Middelburg, A. F. Hofmann, and F. J. R. Meysman (2010), Ongoing transients in carbonate compensation, *Global Biogeochem. Cycles*, *24*, GB4010, doi:10.1029/2009GB003654.

1. Introduction

[2] The current anthropogenic increase in atmospheric CO_2 is foreign to human experience, and its consequences need to be investigated. Over a 100 year time frame, CO_2 uptake will mainly affect the surface layer of the ocean; yet over a 1000 year time frame, this CO_2 will penetrate the deep ocean. Previous studies state that a number of important changes can be expected in the deep-sea carbonate system [e.g., *Zeebe and Westbroek*, 2003; *Archer et al.*, 2009]. One effect is to decrease the amount of $CaCO_3$ that accumulates on the ocean floor, such that what does accumulate, does so at shallower depths. Another effect is the neutralization of the encroaching CO_2 by dissolving previously deposited sedimentary carbonate (PDC), thus permitting natural, long-term sequestration of anthropogenic CO_2.

[3] Our understanding of the effects of CO_2 penetration and consequent acidification of the deep ocean originates from the study and interpretation of the sedimentary record and, just as importantly, through the results of modeling. Study of the geologic record focuses on changes in the accumulation of sedimentary carbonate, and particularly, the positions and vertical migration of so-called critical horizons. During increasing acidification, the saturation depth (z_{sat}), below which the oceans are undersaturated with respect to $CaCO_3$, rises, as do the geochemical carbonate compensation depth (z_{cc}) and the snowline (z_{snow}). The latter two horizons correspond to the depth where the rain of $CaCO_3$ from above exactly balances dissolution at the seafloor and to the depth at which no $CaCO_3$ is present in the sediments, respectively [*Zeebe and Westbroeck*, 2003; *Boudreau et al.*, 2010].

[4] The models employed by oceanographers and geologists aim to reproduce the temporal dynamics of these characteristic horizons. To this end, a variety of carbon cycling models have been employed, ranging from multibox models [e.g., *Keir*, 1988; *Lenton and Britton*, 2006; *Munhoven*, 2007; *Merico et al.*, 2008] to general circulation models with coupled biogeochemistry [e.g., *Archer and Maier-Reimer*, 1994;

[1]Department of Oceanography, Dalhousie University, Halifax, Nova Scotia, Canada.
[2]Geochemistry, Faculty of Geosciences, University of Utrecht, Utrecht, Netherlands.
[3]Netherlands Institute of Ecology, Yerseke, Netherlands.
[4]Monterey Bay Aquarium Research Institute, Moss Landing, California, USA.
[5]Department of Analytical and Environmental Chemistry, Vrije Universiteit Brussel, Brussels, Belgium.

0886-6236/10/2009GB003654

Archer et al., 1998; *Ridgwell and Hargreaves*, 2007; *Archer et al.*, 2009; *Ridgwell and Schmidt*, 2010].

[5] In the present paper we show that the ongoing changes in the saturation depth, z_{sat}, the compensation depth, z_{cc} and the snowline, z_{snow}, and, thus, in the carbonate compensation system, can be modeled easily, rapidly, and quantitatively with a modified Harvardton-Bear model [*Sarmiento and Toggweiler*, 1984; *Siegenthaler and Wenk*, 1984; *Knox and McElroy*, 1984] without a diagenetic submodel. Instead, seafloor $CaCO_3$ dissolution is implemented based on equations by *Boudreau et al.* [2010]. The model is applied to predict the evolution of z_{sat}, z_{cc} and z_{snow} over the next 2000 years, a critical time in acidification, as the input of CO_2 is expected to reach a maximum during this timeframe [*Wigley et al.*, 1996; *Caldeira and Wickett*, 2003].

2. Model

[6] A number of different types of box models have previously been published for the oceanic carbonate system, and so it is appropriate to document how the current model relates to these previous efforts. The original Harvardton-Bear models included three ocean boxes [*Sarmiento and Toggweiler*, 1984; *Siegenthaler and Wenk*, 1984; *Knox and McElroy*, 1984; *Broecker et al.*, 1999; *Archer et al.*, 2000; *Toggweiler et al.*, 2003], which were later followed by even larger multibox models [e.g., *Broecker and Peng*, 1986; *Keir*, 1988; *Stephens and Keeling*, 2000; *Lane et al.*, 2006]. All these box models describe only the carbonate chemistry of the water column, and accordingly, these models contain no feedback from sedimentary carbonate dissolution; therefore, these models are incapable of simulating transient carbonate compensation dynamics, a task for which they were not designed. Moreover, these models have no input of alkalinity from weathering of carbonate and silicate rocks on land, which creates an offset in the ocean-atmospheric CO_2 flux when compared to actual values [*Merico et al.*, 2008]. Recently, *Lenton and Britton* [2006] coupled a 3-box Harvardton-Bear ocean model to a 10-layer diagenetic model of carbonate dissolution, accounting for the input of river alkalinity, while in a similar fashion, *Munhoven* [2007] coupled a 10-box ocean model to a 100-layer diagenetic model. This coupling to an explicit diagenetic model is numerically demanding and substantially increases the computational effort. The main advantage of the ocean box model proposed here is that it implements a novel parameterization of sedimentary carbonate dissolution [*Boudreau et al.*, 2010], which makes an explicit diagenetic model unnecessary. Finally, *Archer et al.* [2009] have shown that the single-box GEOCARB/GEOCYC model [*Berner and Kothavala*, 2001] generates inaccurate CO_2 fluxes on the time scale of interest to this paper.

[7] Figure 1 displays a schematic of our 4-box model (L = low-latitude surface layer; H = high-latitude surface layer; D = deep ocean; A = atmosphere). All boxes are considered internally well mixed. Our novel parameterization of seafloor $CaCO_3$ dissolution in the deep ocean box (further details below) uses the actual ocean bathymetry. The differential bathymetric curve $a'(z)$ is derived from the ETOPO1 global relief model of Earth's surface [*Amante and Eakins*, 2009]. The sediment area between two water depths, $A(z_2,z_1)$, is then calculated as the integral

$$A(z_2, z_1) = \int_{z_1}^{z_2} a'(z)dz \tag{1}$$

where $z_2 > z_1$. The total ocean area A_D is calculated by setting $z_1 = 200$ m and $z_2 = 10898$ m, i.e., the maximal depth of the ocean (z_{max}). By using the 200 m isobath, we exclude the coastal ocean and continental shelves. The model geometric parameters are summarized in Table 1.

[8] The model explicitly simulates the dynamics of dissolved inorganic carbon, $[\Sigma CO_2]$, and total alkalinity, [TA], within each ocean box in Figure 1, plus the pCO_2 of the atmosphere. From these values, seawater pH is calculated using a standard acid-base equilibration procedure, calculated on the "free" scale using equilibrium expressions from *Millero et al.* [2006]. An important extension in our model is that it explicitly simulates the time evolution of the saturation depth, z_{sat}, the compensation depth, z_{cc}, and the snowline, z_{snow}, within the deep-ocean box, thus adding three extra state variables. These new state variables are resolved with the equations given by *Boudreau et al.* [2010]. The saturation horizon is calculated as

$$z_{sat} = z^0_{sat} ln\left(\frac{[Ca^{2+}][CO_3^{2-}]_D}{K^0_{sp}}\right) \tag{2}$$

where $[Ca^{2+}]$ is the oceanic calcium concentration (taken to be constant across all three boxes), K^0_{sp} is the solubility product of calcite at the air-water interface, and z^0_{sat} is a characteristic depth (Table 2). Once the alkalinity and DIC values in the deep-ocean box are known, the carbonate concentration, $[CO_3^{2-}]_D$, can be calculated from the governing acid-base equilibria in seawater, and equation (2) provides z_{sat}. Similarly, the carbonate compensation depth, z_{cc}, is given by [*Boudreau et al.*, 2010]

$$z_{cc} = z^0_{sat} ln\left(\frac{B[Ca^{2+}]}{K^0_{sp} A_D k_c} + \frac{[Ca^{2+}][CO_3^{2-}]}{K^0_{sp}}\right) \tag{3}$$

where B is the export of calcite into the deep ocean box, and k_c denotes a heterogeneous rate constant/mass transfer coefficient for calcite dissolution. (Aragonite is explicitly ignored as a second-order contribution.) Again, all quantities in equation (3) are known a priori, except for the carbonate ion concentration, which can be calculated from our model at each time step. Finally, the movement of the snowline, z_{snow}, is given by the differential equation

$$\frac{dz_{snow}}{dt} = -\frac{B_{PDC}(t)}{a'(z_{snow}(t)) I_{CaCO_3}} \tag{4}$$

where $a'(z)$ is the differential bathymetric curve, see equation (1), I_{CaCO_3} is the inventory of dissolvable $CaCO_3$ (in mol m^{-2}) stored in the sediment above the saturation depth, and $B_{PDC}(t)$ represents the dissolution rate of previously deposited carbonate (as calculated below). Equation (4)

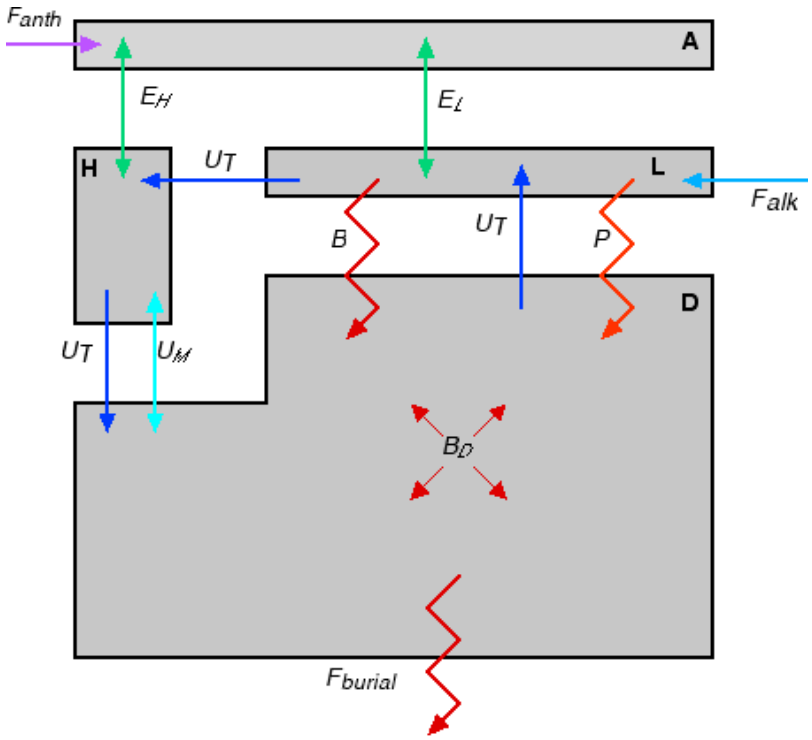

Figure 1. The modified Harvardton-Bear 3-box model for the carbonate system of the oceans. The ocean is divided into 3 boxes for the low-latitude surface (L), high-latitude surface (H) and deep (D) waters. There is also an atmosphere (A) with a prescribed (time varying) emissions-based input. Water flows come from thermohaline circulation (U_T) and mixing (U_M), and there is an external flow of alkalinity and DIC as HCO_3^- from rivers (F_{alk}). Production of solid $CaCO_3$ and organic matter in Box L that are transferred to the deep water are given by B and P, respectively. $CaCO_3$ is regenerated at a rate B_D, while all the organic matter is regenerated. There is also CO_2-gas exchange, E_H and E_L, between the atmosphere and Boxes H and L, respectively. Finally there is burial of calcite, F_{burial}. Assumed and calculated values of parameters and variables for the preindustrial state are given in Tables 1–4.

is the differential form of the equation given by *Boudreau et al.* [2010]; it is employed because it is easier to solve equation (4) than its integral form. The value of I_{CaCO_3} is taken constant and is derived using typical values for the porosity (0.8), a surface sediment mixing depth (10 cm), and a global mean carbonate fraction of sediments above the snowline (0.50).

[9] In contrast to some earlier versions of the Harvardton-Bear model [*Sarmiento and Toggweiler*, 1984; *Siegenthaler and Wenk*, 1984; *Toggweiler et al.*, 2003], we include a net input of DIC and carbonate alkalinity, as an HCO_3^- flux from rivers/coastal oceans into the surface ocean box, i.e., F_{alk} [e.g., *Lenton and Britton*, 2006; *Merico et al.*, 2008]. As a consequence, at steady state, the model buries, on a mole basis, half of F_{alk} as solid $CaCO_3$ and returns the other half as a flux of CO_2 to the atmosphere. This constitutes the oceanic part of the global CO_2 weathering cycle. In addition, the export rates of calcite, B, and organic matter, P, to the deep-ocean box are treated separately, because these rates may change independently with ocean acidification, i.e., a calculated, rather than fixed, rain ratio. No organic matter is buried in our model and the model assumes that DOC, POC, and PIC from rivers are intercepted in the coastal ocean before reaching our surface boxes.

Table 1. Geometrical Model Parameterization

Parameter	Units	Box H	Box L	Box D
Height	m	350	100	3852
Surface area	m^2	0.50×10^{14} (15%)	2.85×10^{14} (85%)	3.36×10^{14}
Volume	m^3	1.76×10^{16}	2.85×10^{16}	1.29×10^{18}
Temperature	°C	2	21.5	2
Pressure	bar	17.6	5.0	240
Salinity	-	35	35	35

Table 2. Biogeochemical Rate Parameters

Parameter	Symbol	Units	Value
Piston velocity	v_G	m d^{-1}	4.8
$CaCO_3$ dissolution coefficient[a]	k_c	m yr^{-1}	8.84
$CaCO_3$ solubility at interface	K_{sp}^0	mol^2 kg^{-2}	4.29E-07
Characteristic depth	z_{sat}^0	m	5078
Ca^{2+} concentration	$[Ca^{2+}]$	mol kg^{-1}	0.0103
$CaCO_3$ inventory	I_{CaCO3}	mol m^{-2}	529
CO_2 fertilization constant	$f_{CO2fert}$	atm^{-1}	600

[a]Calculated from *Boudreau et al.* [2010, equation 3].

[10] A salient feature of our model is its description of the fate of the calcium carbonate that is exported to the deep ocean. Part of this carbonate is dissolved, at rate B_D, while the remainder is buried within the sediment, at rate F_{burial}, i.e.,

$$B = B_D + F_{burial} \tag{5}$$

We distinguish four different types of dissolution, so that the total dissolution B_D has four components

$$B_D = B_{DS} + B_{CC} + B_{NS} + B_{PDC} \tag{6}$$

where B_{DS} = dissolution of $CaCO_3$ raining down between z_{sat} and z_{cc}, which is driven by undersaturation, as well as by aerobic respiration within sediment; B_{CC} = dissolution of $CaCO_3$ raining down on the sediment-water interface below z_{cc}, which is not an explicit function of the saturation, but only depends of the hypsography [e.g., *Merico et al.*, 2008]; B_{NS} = dissolution of more soluble $CaCO_3$ (aragonite, high-Mg calcite, etc.) above z_{sat}, plus dissolution driven by aerobic respiration within sediments; finally B_{PDC} = transient dissolution of previously deposited solid carbonate between z_{snow} and z_{cc}. The burial rate is always calculated by difference between calcite export and dissolution, i.e., $F_{burial} = B - B_D$. This implies that, in a transient situation with strong dissolution of previously deposited carbonate, the burial rate can become negative. The dissolution rate B_{DS} will depend on depth, as the degree of undersaturation increases with depth; thus, close to z_{cc}, this dissolution will nearly match the rain rate, while close to z_{sat}, this dissolution will tend to B_{NS}.

[11] Below the compensation depth, z_{cc}, the potential for dissolution exceeds the rain of $CaCO_3$ to the seafloor [e.g., *Merico et al.*, 2008]. As a result, the dissolution rate below z_{cc} is not an explicit function of the saturation state, but only depends of the hypsography,

$$B_{CC} = \frac{A(z_{cc}, z_{max})}{A_D} B \tag{7}$$

where A_D is the total area of the seafloor, i.e., $A(z_{max},z_o)$. Above the saturation horizon, z_{sat}, calcite dissolution will occur that is driven by oxic respiration in sediments. This dissolution is treated as proportional to the sediment surface area above the saturation horizon

$$B_{NS} = \alpha_{RD} \frac{A(z_0, z_{sat})B}{A_D} \tag{8}$$

The coefficient α_{RD} (ranging between 0 and 1) defines the fraction of calcite that is dissolved above the saturation horizon by respirational dissolution, and its value is obtained from calibration of the steady state at preindustrial conditions (as discussed in section 3).

[12] The dissolution rate B_{DS} between the saturation horizon and the compensation depth consists of two components, a part driven by undersaturation ($B_{DS}^{undersat}$), and a part driven by respirational dissolution (B_{DS}^{resp}). As argued in section 3, the dissolution of $CaCO_3$ is principally controlled by mass transfer at the sediment-water interface, and consequently, $B_{DS}^{undersat}$ is driven entirely by the degree of undersaturation in the overlying seawater at a given location (and hence not in the sediment). In this way, one can adopt a simplified kinetic rate description that no longer requires an explicit spatial description of the sediment column, i.e.,

$$B_{DS}^{undersat} = k_c \int_{z_{CC}(t)}^{z_{sat}(t)} a'(z)\left(C_{sat}(z,t) - [CO_3]_D(t)\right)dz \tag{9a}$$

where k_c is the heterogeneous rate constant/mass transfer coefficient for seafloor dissolution (units of length per unit time) and $a'(z)$ is the differential hypsographic curve, equation (1).

[13] On the other hand, B_{DS}^{resp} is calculated as proportional to the fraction of the incoming flux that is not dissolved

$$B_{DS}^{resp} = \alpha_{RD}\left(\frac{A(z_{sat}, z_{CC})B}{A_D} - B_{DS}^{undersat}\right) \tag{9b}$$

The coefficient α_{RD} (ranging between 0 and 1) is the same as in equation (8). This ensures that the total dissolution flux changes in a continuous fashion with water depth.

[14] The fourth and final component of B_D comes from the dissolution of previously deposited $CaCO_3$. This exists only in the transient case. It is treated again as a first-order process,

$$B_{PDC} = k_c \int_{z_{snow}(t)}^{z_{CC}(t)} a'(z)\left(C_{sat}(z,t) - [CO_3]_D(t)\right)dz \tag{10}$$

where k_c is the rate constant/mass transfer coefficient for seafloor dissolution introduced above, and $z_{cc}(t)$ and $z_{snow}(t)$ are obtained from equations (2) and (3).

[15] The final processes that need to be specified are the warm and cold ocean surface gas exchange rates (flows), E_L and E_H, respectively. This is done by assuming simple gas exchange laws; specifically, for the warm surface ocean,

$$E_L = v_G A_L\left([CO_2]_L - [CO_2]_{atm}\right) \tag{11}$$

where $[CO_2]_L$ is the CO_2 concentration in Box L, as calculated from the ΣCO_2 and total alkalinity from the model, $[CO_2]_{atm}$ is the concentration at equilibrium with the atmosphere, v_G is a piston velocity (4.8 m d^{-1}) [*Sarmiento and Gruber*, 2006], and A_L is the area of the low-latitude ocean. The cold ocean version of equation (11) is operationally identical.

3. Preindustrial Steady State

[16] Parameter values in the model are set by fitting our model to preindustrial ocean conditions. Table 1 lists the geometric parameter values used in these calculations. Tables 2–4 list the variable and parameter values used to characterize the preindustrial ocean or obtained by fitting those preindustrial conditions. In particular, the preindustrial concentration data are consistent with *Key et al.* [2004]. The carbonate rain B is set to 60 Tmol yr^{-1}. The rate of organic

Table 3. Preset Values of State Variables in Preindustrial Steady State

Parameter	Units	Box H	Box L	Box D
ΣCO_2	mol kg^{-1}	2153	1952	2291
Alkalinity	mol kg^{-1}	2345	2288	2399
pH	-	8.22	8.26	7.91
$[CO_3^{2-}]$	mol kg^{-1}	138	234	86
Saturation state	-	3.18	5.56	1.30
z_{sat}	m			3715
z_{cc}	m			4750
z_{snow}	m			4750

matter rain to the deep sea, P, is taken to be 200 Tmol yr^{-1}, and the resulting initial rain ratio, B/P, is then 0.3.

[17] In addition, using the above B value, an ocean-area weighted z_{cc} of 4750 m from the data given by *Broecker and Peng* [1982], and the z_{cc} formula given by *Boudreau et al.* [2010], a value of the rate constant for $CaCO_3$ dissolution k_c of 8.83 m yr^{-1} is obtained; this value is remarkably close to the mean value for the mass transfer coefficient, k_T, for calcium/carbonate ion at the seafloor, i.e., 9.65 m yr^{-1}, as calculated from *Boudreau* [2001]. This finding supports the contention that seafloor calcite dissolution is mass transfer controlled [e.g., *Oxburgh*, 1998; *Broecker*, 2008, 2009; *Boudreau et al.*, 2010] (see also Text S1).[1] (Note that *Boudreau et al.* [2010] cite a k_c of 7 m yr^{-1}, but that was produced using an earlier version of the current model and slightly different inputs.)

4. Future Ocean

4.1. Preliminary Calculations

[18] To assess the performance of our new model in describing the long-term fate of fossil CO_2, we compared our simulation output to that from the Long Tail Model Intercomparison Project (LTMIP), which includes 8 different models of varying complexity, including Earth system models with a full biogeochemistry and carbon cycle capabilities: see *Archer et al.* [2009] for details. LTMIP involved a series of numerical fossil fuel neutralization experiments, in which pulses of 1000 or 5000 Pg C are liberated to the atmosphere and the subsequent invasions of CO_2 into the ocean and their interactions with carbonate sediments are simulated. Our model results are compared for the situation where only the chemistry of the ocean water column responds to CO_2 invasion, i.e., the base run given by *Archer et al.* [2009], and for the simulations that additionally include feedback from sedimentary carbonate dissolution, i.e., the S simulations given by *Archer et al.* [2009].

[19] Our fossil fuel neutralization simulation results compare favorably to the benchmark outputs reported in LTMIP. The equilibration time for CO_2 invasion into the ocean was calculated by a least squares fit of an exponential curve to the atmospheric CO_2 trajectory of the base run. Our values are 218 and 430 years for the 1000 and 5000 Pg C spikes, respectively, which are close to the mean of the LTMIP ranges, i.e., 250 ± 90 and 450 ± 200 years, respectively. The airborne fraction, i.e., the fraction of the initial CO_2 spike that remains in the atmosphere, is 24.4% (base run) and 16.0% (S run) after 10,000 years in the 5000 Pg C release experiment, while the LTMIP range for the CS runs is 13–32%. Similarly, the airborne fraction in the 1000 Pg C release experiment becomes 10.5% and 8.6% after 10,000 years for the base and S runs, respectively, whereas the LTMIP range for the CS runs is 10–20%. (Note that the LTMIP only reports "CS" runs, which combine the feedback of climate [C] and sediment [S], while our model only addresses the sediment [S] effect. The climate feedback typically increases the airborne fraction by ~5% [see *Archer et al.*, 2009, Figures 3a and 4a], such that after adding this climate effect to our S run results, our predicted airborne fraction would fall in the center of the LTMIP range.)

4.2. IS92a Results

[20] Given the preindustrial parameter values and assuming that calcification (B), primary production (P), weathering (F_{alk}) and the temperature of the boxes remain constant, it is possible to force the model by the CO_2 emission scenario in Figure 2. The emissions curve describes the input of CO_2 to the combined atmosphere-ocean system, hence discounting land uptake; this explains why the model forcing in Figure 2a is slightly lower than the data based on estimated fossil fuel emissions. The emission scenario follows the IPCC IS92a projection for the 21st century (Figure 2b), and uses a Gaussian evolution afterward, which peaks near the year 2250 AD. The total emission is 4025 Gt C over a period of 600 years, which leads to maximum atmospheric CO_2 concentrations of around 1400 ppm (Figure 2b). The model was integrated from the year 1800 AD to 3800 AD. Figure 3 illustrates the predicted evolution of the state variables, i.e., concentrations, saturation states and the horizon depths (z_{sat}, z_{cc} and z_{snow}), while Figure 4 displays the molar flows in the model, over this same integration period. The results in Figures 3 and 4 are termed the "Base Model" hereafter.

[21] The $\acute{O}CO_2$ (Figure 3a) increases rapidly in the surface ocean boxes during the period 1900–2250 AD, and slowly rises thereafter, even while the atmospheric CO_2 falls, because of upwelling of CO_2-enriched deep water from

Table 4. Preindustrial Steady State: Geochemical Rates

Parameter	Symbol	Units	Value
	U_T	Sv	25[a]
	U_M	Sv	30[a]
	P	Tmol C yr^{-1}	200[a]
	F_{alk}	Tmol C yr^{-1}	24[a]
	E_H	Tmol C yr^{-1}	+33
	E_L	Tmol C yr^{-1}	−45
Calcification	B	Tmol C yr^{-1}	60[a]
	B_{NS}	Tmol C yr^{-1}	19.1
	B_{DS}	Tmol C yr^{-1}	10.4
	B_{CC}	Tmol C yr^{-1}	18.6
	B_{PDC}	Tmol C yr^{-1}	0
	B_D	Tmol C yr^{-1}	48
	F_{burial}	Tmol C yr^{-1}	12
Rain ratio (calculated)	RR	-	0.3

[a]Preset values.

[1]Auxiliary materials are available in the HTML. doi:10.1029/2009GB003654.

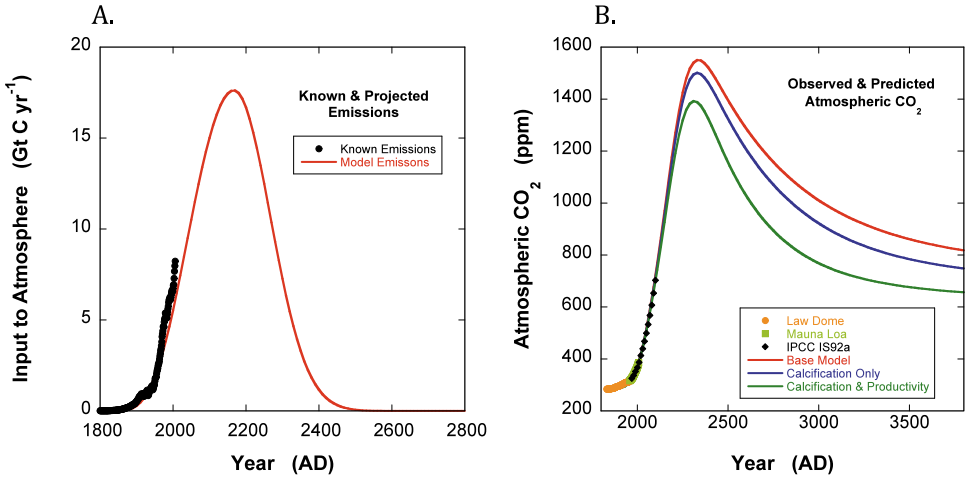

Figure 2. Diagram A illustrates the IS92a CO_2 emission scenario used to force our model. Diagram B is the simulated atmospheric CO_2 concentration.

Box D. Total alkalinity (Figure 3b) barely changes in the initial 350 year period, but increases in all the boxes quasi-linearly, thereafter. The initial introduction of CO_2 from the atmosphere causes no change in alkalinity, but as the anthropogenic CO_2 reacts with sedimentary calcite in the deep box, and this water upwells, the alkalinity in each box will increase in tandem. The pH (Figure 3c) in all boxes drops initially with acidification from anthropogenic CO_2, but reaction with sedimentary calcite over the later 2000 years neutralizes this increase, and eventually, the upwelling of deep, high-alkalinity water allows the pH of the surface oceans to partially recover. The pH trends are mirrored in the calcite saturation state, Omega (Figure 3d), as expected. (Omega = $[CO_3^{2-}]_{Box}/[CO3_3^{2-}]_{sat}$).

[22] The positions of the critical horizons are shown in Figure 3e. The saturation depth, z_{sat}, rises rapidly in response to the introduction of anthropogenic CO_2, reaching the top of the deep-water box by 2550 AD. Neutralization via sedimentary calcite dissolution does not act sufficiently on this time scale to stop the transient rise in z_{sat}. The result is a "runaway" increase in the undersaturation of the deep ocean. In contrast, while the calcite compensation depth, z_{cc}, rises in parallel, it fails to reach the top of Box D before neutralization starts to curb and reverse its rise. The result is a substantial separation in z_{sat} and z_{cc}, i.e., as much as 1700 m by 2550 AD, as predicted by *Boudreau et al.* [2010]. The snowline, z_{snow}, moves up about 1150 m during the course of the simulation; thus the sediments would experience observable effects from calcite dissolution [*Roberts and Tripati*, 2009] in that period. These simulations argue that the projected acidification, with the magnitude and timing driven by the IS92a scenario (Figure 2), would cause large changes in benthic compensation dynamics, as well as a transient disconnection between the positions of the critical carbonate horizons.

[23] The flows/transfer rates of carbon in Figure 4a show that CO_2 enters the ocean in both the high- and low-latitude boxes after 1955 AD, but this timing is dependent on the assumed proportion of the surface ocean occupied by these boxes. CO_2 input reaches a maximum near 2250 AD. From the gas transfer data, we calculate that the average influx of anthropogenic CO_2 for the period 1990–1999 would be about 1.75 Pg yr^{-1}; this estimate is in line with that from the CC_SED model [*Archer*, 2005], and within the range of values listed by *Gruber et al.* [2009], i.e., 2.2 ± 0.4 Pg C yr^{-1} (via inversion) and 1.9 ± 0.7 Pg C yr^{-1} (via p_{CO2}-climatology), and *Khatiwala et al.* [2010], i.e., 2.0 ± 0.6 Pg C yr^{-1}. As stated above, *Archer et al.* [2009] present results from the LTMIP, which involved 9 models that resolve the long-term fate of fossil fuel carbon and include a sediment carbonate module. Excluding the two extremes of less than 1 and more that 3 Pg C yr^{-1}, these models generate anthropogenic carbon uptake values ranging between 1.55 and 2.5 Pg C yr^{-1} for the period 1990–2000, which is consistent with the prediction from our simple box model.

[24] Figure 4b records that the burial of calcite will reverse with time to a large net loss (via dissolution of previously deposited $CaCO_3$), as compared to the preindustrial positive accumulation rate. With the rise in z_{sat} and the development of undersaturation everywhere in the oceans, nonsaturation related dissolution above z_{sat}, B_{NS}, will fall both in magnitude and importance. The concurrent rise in z_{cc} will mean that saturation-state-dependent dissolution, B_{DS} given by equation (9a), will also drop in magnitude and importance. Conversely, hypsographic-dependent dissolution below z_{CC}, B_{CC}, and the dissolution of previously deposited calcite, B_{PDC}, will both increase dramatically (Figure 4c). B_{PDC} will decrease as the snowline z_{snow} begins to rise, but B_{CC} will remain essentially constant until at least 3800 AD.

[25] Our model predicts a negative burial flux (i.e., sediment carbonate dissolution flux) of ~ −50 Tmol C yr^{-1} or ~ −0.6 Pg C yr^{-1} (Figures 4a and 4b) by the year 2500. In comparison, LTMIP results [*Archer et al.*, 2009] also predict burial fluxes for simulations with a pulsed release of 5000 Pg C; these model predictions are rather disparate, as burial fluxes after 500 years range from close to zero to ~ −1.2 Pg C yr^{-1}. In particular, our box model generates

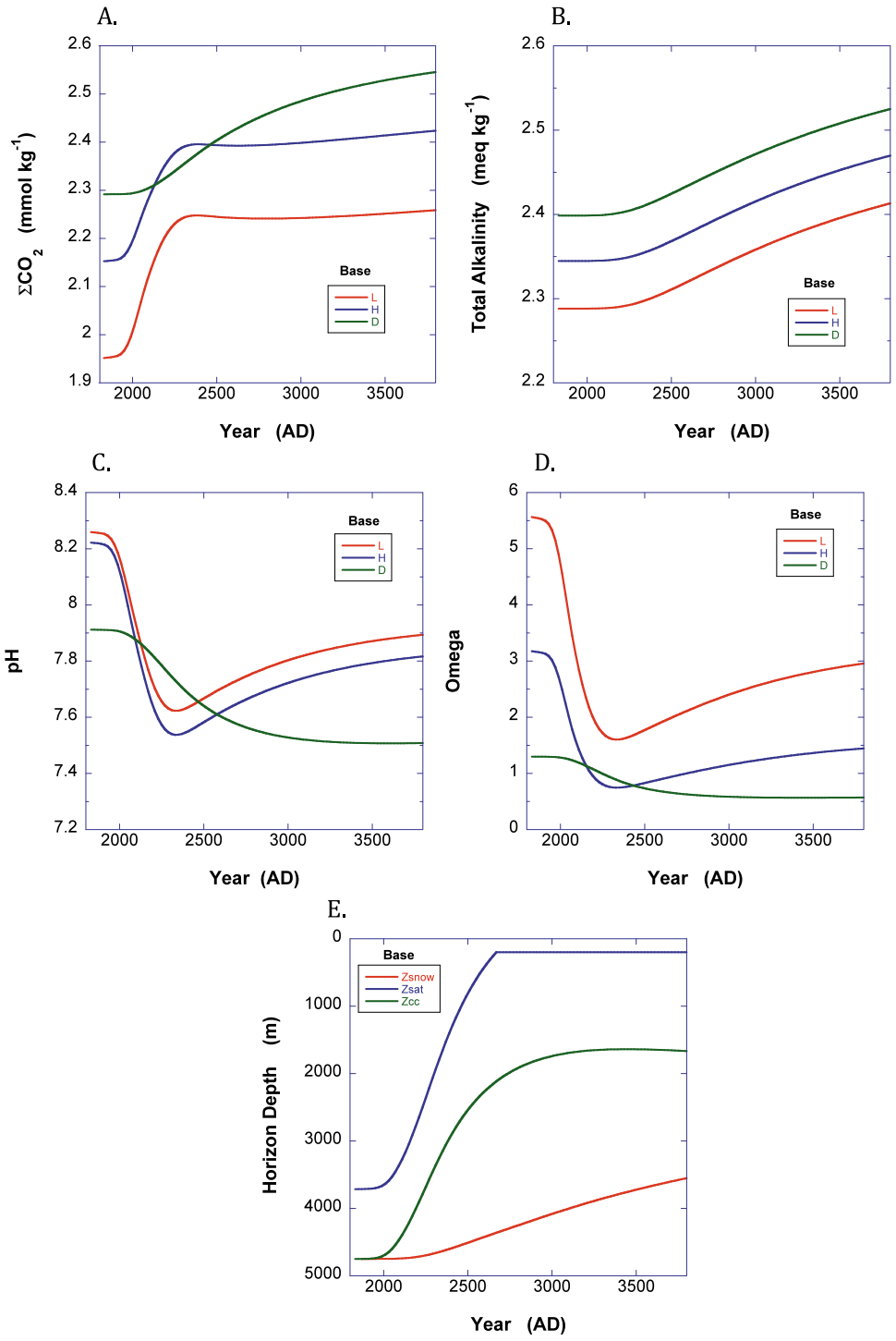

Figure 3. Predicted evolution of concentrations and critical carbonate horizons with the IS92a CO_2 scenario from Figure 2. (a) Total dissolved CO_2, (b) total alkalinity, (c) pH, (d) saturation state, Omega = $[CO_3^{2-}]/[CO_3^{2-}]_{sat}$, and (e) position of the critical horizons: z_{snow}, snowline; z_{sat}, calcite saturation horizon; and z_{cc}, carbonate (calcite) compensation depth. (See *Boudreau et al.* [2010] for precise definitions of these horizons.)

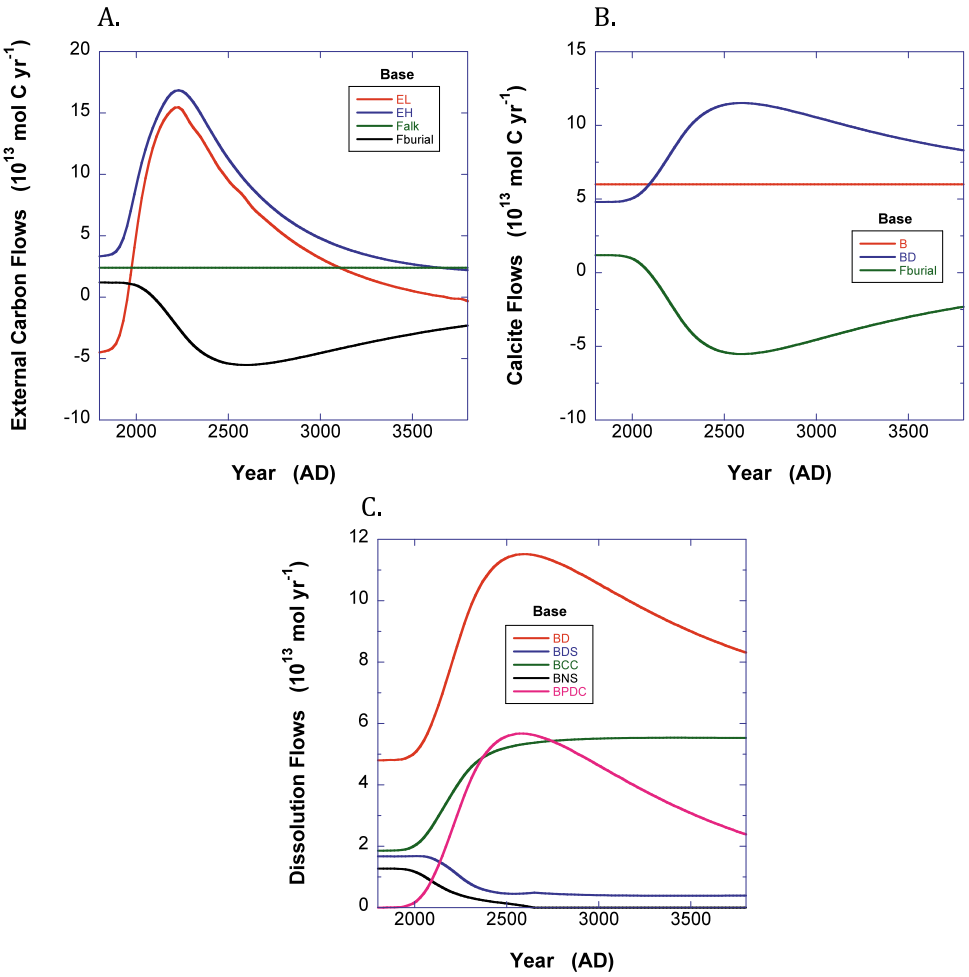

Figure 4. Predicted evolution of the molar C exchange rates/flows. E_L and E_H are the gas flows between the atmosphere and the low (L) and high (H) latitude boxes, respectively. F_{alk} is the flow of carbonate alkalinity from the rivers, and F_{burial} is the burial flow. B is the production of calcite in Box L and B_D is the total dissolution rate of calcite in the deep ocean (Box D). Dissolution components are: B_{PDC} = transient dissolution of previously deposited $CaCO_3$ in the sediments between z_{cc} and the *snowline*, B_{CC} = dissolution of $CaCO_3$ raining down to the seafloor between z_{cc} and the bottom of deep ocean (Box D), B_{NS} = largely metabolically driven dissolution in the deep ocean, and B_{DS} = dissolution of $CaCO_3$ raining down to the seafloor between z_{cc} and z_{sat}.

negative burial fluxes similar in magnitude and temporal evolution to the CC_Sed model [*Archer*, 2005; *Archer et al.*, 2009].

[26] At this point one is drawn to ask why such a coarse physical model as our modified Harvardton-Bear can produce (at least some) results similar to far more sophisticated and highly resolved models? For example, the Havardton-Bear models assume that the deep sea is homogenized by mixing, but that is strictly true only on time scales greater than the water residence time, i.e., about 1000 years. Another crude approximation in Harvardton-Bear relates to the pycnocline. Ideally, the parts of the oceans represented by boxes are internally well mixed and separated by relatively "thin" boundary/transition zones, in which gradients are concentrated. The pycnocline does concentrate the transitional gradients between surface and deep boxes, but it is also much thicker than the surface box; thus some approximation must be made to assign the pycnocline volume to a box, i.e., in our case to the deep box. Moreover, the effects of sources and sinks internal to the pycnocline also need to be redistributed. Overall, what our results indicate is that accurate functional forms for the controlling physicochemical processes, i.e., $CaCO_3$ dissolution, and consistent estimates of rates of all processes are more important in obtaining correct, first-order, ocean-integrated, carbonate system dynamics than detailed spatial resolution of the physical transport processes.

[27] The above findings and arguments further beg the question of the importance of differentiating/partitioning the carbonate dissolution processes, based on the positions of the critical horizons, as we have done. We establish the importance of dissolution partitioning by comparing the

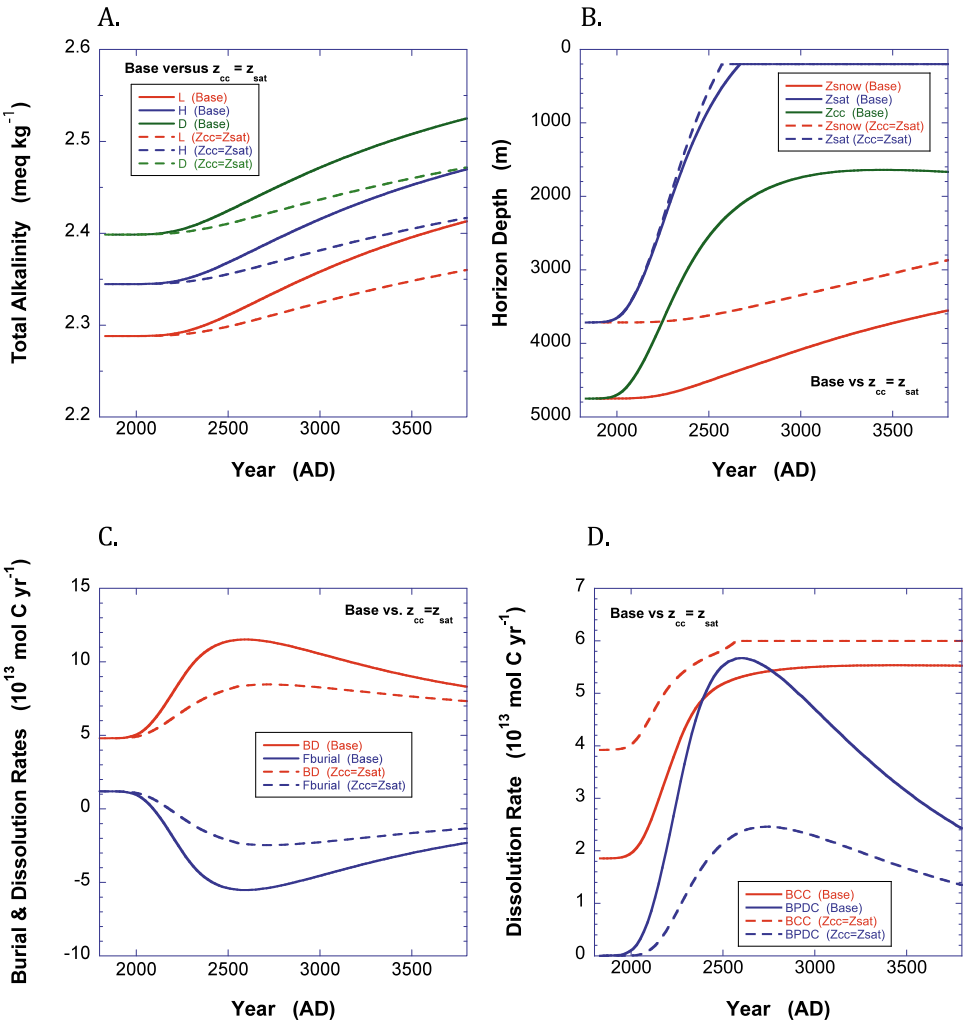

Figure 5. Illustration of the significant differences between the predictions from the Base Model (Figures 3 and 4) and a model that assumes that the saturation and compensation horizons are the same, i.e., $z_{cc} = z_{sat}$. Diagrams A and B compare the ΣCO_2 and Total Alkalinity, respectively. Diagram C contrasts the rate of $CaCO_3$ dissolution and burial in the deep ocean box, while Diagram D contrasts the rates of $CaCO_3$ dissolution below the compensation depth (z_{cc}) and the dissolution of previously deposited carbonate.

results in Figures 3 and 4 with the results of an otherwise identical model, but where all dissolution occurs at the saturation horizon, i.e., $z_{cc} = z_{sat}$, and where z_{snow} is initially at z_{sat}. This approximation is often used in paleoceanographic models, although this is patently not the case in the present oceans; that is, there exists a z_{cc}–z_{sat} separation of ~850 m. Our comparative results are given in Figure 5.

[28] First, all oceanic boxes have higher alkalinity in our Base Model than with the assumption that $z_{cc} = z_{sat}$, i.e., by about 0.05 meq kg^{-1} at the end of the integration period (Figure 5a). This indicates that there is less dissolution of $CaCO_3$, particularly of previously deposited carbonate, in the $z_{cc} = z_{sat}$ model. The $z_{cc} = z_{sat}$ scenario exaggerates the rise of the compensation depth by as much as 1.5 km (Figure 5b), and the snowline is 0.8 km too shallow. Calcite dissolution and burial rates are significantly smaller in the $z_{cc} = z_{sat}$ model (Figure 5c); likewise, the components and magnitude of the dissolutive rate are significantly different in the $z_{cc} = z_{sat}$ model, e.g., dissolution below the (misplaced) compensation depth is highly exaggerated and the dissolution of previously deposited carbonate is similarly underestimated (Figure 5d). While a $z_{cc} = z_{sat}$ model represents a convenient approximation, there are fundamental variances from our Base Model, and we view these differences as inaccuracies.

[29] Paleoceanographic models of the effects of past changes in atmospheric CO_2 on carbonate compensation dynamics often assume that $z_{cc} = z_{sat}$ [e.g., *Merico et al.*, 2008; *Roberts and Tripati*, 2009]. Our findings imply that ignoring this distinction between saturation and compensation depths in paleoceanographic modeling may underestimate dissolution of sedimentary carbonates and steady state depths of z_{cc} and z_{snow}, and, thus, in reconstructed snow line

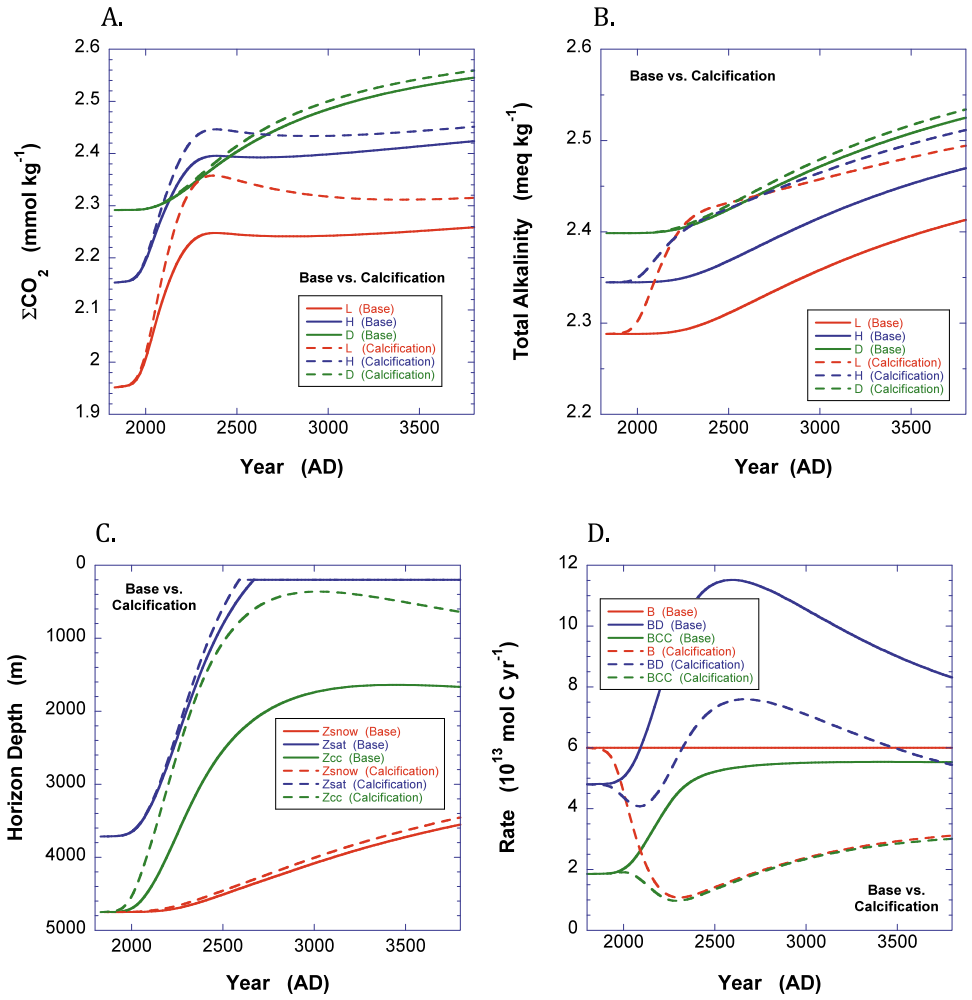

Figure 6. The effect of adding a feedback, equation (12), on the export production of $CaCO_3$ (B). Diagrams A and B compare the $\acute{O}CO_2$ and Total Alkalinity of the Base Model and the calcification feedback model, respectively. Diagram C illustrates the difference in the behaviors of the critical carbonate horizons. Diagram D contrasts the rates of $CaCO_3$ production (B), total dissolution in the deep box (B_D) and dissolution below the carbonate compensation depth, z_{cc}.

excursions. Past carbon input events are quantified by the shoaling of the snow line, and the steady state position of the z_{cc} before acidification events is as critical as the actual shoaling [*Zeebe et al.*, 2009].

[30] A potentially important omission in our Base Model is any feedback on carbonate or organic matter productivity in the surface ocean (Box L) as a consequence of changing carbonate chemistry [*Gehlen et al.*, 2007]. Both B and P were treated as constant in our model and the calculations by *Boudreau et al.* [2010]. As the B and P input rates to the deep ocean are prominent pieces of benthic compensation dynamics, this omission needs to be explored.

[31] The potential negative feedback between calcite production and the falling saturation state of the surface waters due to CO_2 uptake can be modeled as a linear function of the saturation difference, i.e.,

$$B = B^{ref}\frac{\Omega_L - 1}{\Omega_L^{ref} - 1} \qquad (12)$$

where B^{ref} and the saturation state Ω_L^{ref} are the preindustrial steady state values. As surface water acidifies, equation (12) causes a drop in the input rate of calcite to the deep-ocean box.

[32] The differences caused by adding a calcification feedback are illustrated in Figure 6. Feedback to calcification allows more $\acute{O}CO_2$ to remain in the surface oceans and causes only a small change in deep ocean $\acute{O}CO_2$ over the integration period (Figure 6a). The evolution of surface total alkalinity, however, changes radically; as the saturation state of the surface waters falls, the removal of alkalinity also falls, and alkalinity builds up in the surface boxes to mirror the deep-ocean value (Figure 6b). In contrast, the deep ocean gains only a small increase in alkalinity (~0.01 meq kg^{-1}). Changes in pH and calcite saturation state (Omega) are modest between these simulations and the rise in the saturation horizon, z_{sat}, is almost identical. What does change is the evolution of the compensation depth, z_{cc}: it rises faster and nearly reaches the base of the surface layer before

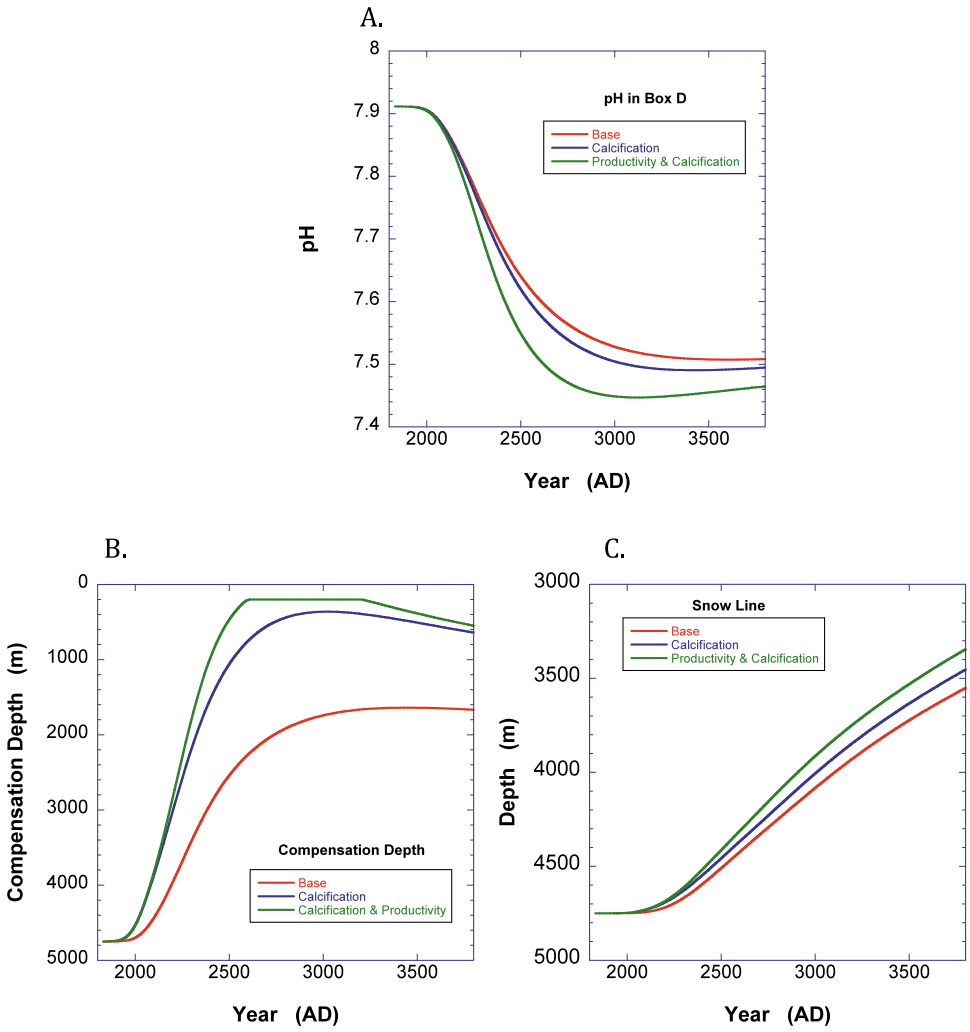

Figure 7. Comparison of the predicted pH (Diagram A), compensation depth, z_{cc} (Diagram B), and snowline (Diagram C) for the Base Model and for that model with added calcification feedback, equation (12), and with both calcification and organic matter productivity feedbacks, equations (12) and (13).

falling (Figure 6c). The position of z_{cc} depends directly on B (see equation (3)), and the fall in B with acidification is enough to cause this horizon to rise significantly more than in the Base Model. Finally, the rates of the different dissolution processes are also altered (Figure 6d). Total dissolution of $CaCO_3$ is lower than in our Base Model, again reflecting the fall in $CaCO_3$ production (B); likewise, dissolution below the compensation depth also falls to mirror the fall in B, because it too depends directly on B, i.e., equation (12).

[33] The suggested role of carbonate-production feedback on benthic compensation dynamics indicates that the nature of this process needs to be clarified and that the magnitude of this feedback should be accurately quantified and parameterized. It also has implications to paleoceanographic studies. If a strong feedback is possible, then during acidification, z_{cc} will approach z_{sat}, contrary to statements by *Boudreau et al.* [2010], because that previous study assumed B to be constant. Understanding of the critical carbonate depth in past oceans is dependent on clarification of this issue.

[34] We also simulated the effect of relating the organic matter productivity to $[CO_2]_L$ using the parameterization of *Riebesell et al.* [2007], i.e.,

$$P = P_{ref}\left(1 + f_{CO2fert}\left([CO_2]_L - [CO_2]_L^{ref}\right)\right) \qquad (13)$$

where f_{CO_2fert} represents the strength of the CO_2 fertilization effect, while P_{ref} and $[CO_2]_L^{ref}$ are the primary production and dissolved carbon dioxide in the preindustrial steady state.

[35] The productivity feedback from equation (13) causes a long-term additional decrease in the pH of the deep water (Figure 7a), if all the organic matter is regenerated in this box. The lower pH causes the compensation depth, z_{cc}, to rise all the way to the top of the deep ocean box (Figure 7b). It also causes a small additional rise in the snowline (Figure 7c). A

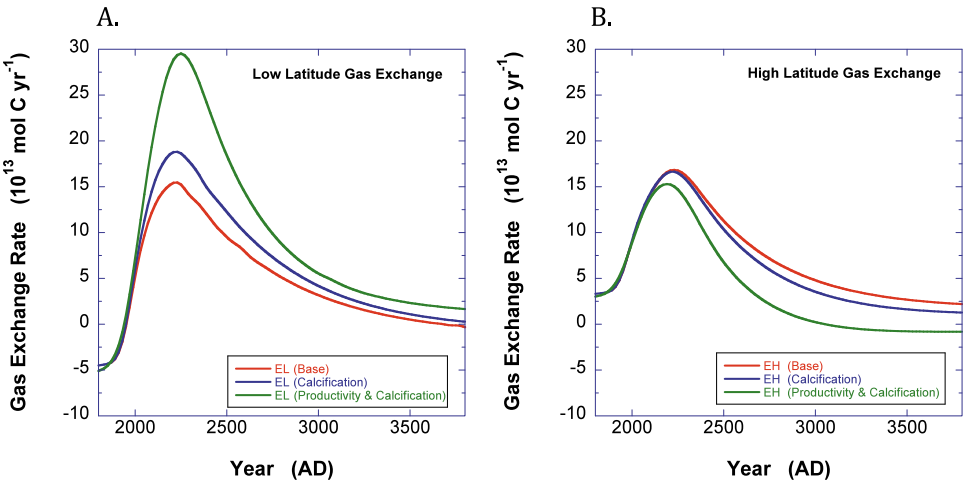

Figure 8. Comparison of the prediction of gas exchange rates in the low-latitude ocean, Box L (Diagram A), and in the high-latitude ocean compensation depth, Box H (Diagram B) for the Base Model, and for that model with added calcification feedback, equation (12), and with both calcification and organic matter productivity feedbacks, equations (12) and (13).

signal effect from productivity feedback is a dramatic increase in the gas exchange rate in the low-latitude box (Figure 8), as biological demand increases. There is a corresponding small decrease in gas exchange in the high-latitude ocean, as the waters moving into Box H from Box L are now more saturated. The additional effects of productivity feedback on ocean composition are generally modest. Note however that the productivity feedback implemented is an acute extrapolation, far beyond the 21st century horizon of *Riebesell et al.* [2007]. This extrapolation implies a large and continuous increase in the C/N and C/P ratios of the organic matter exported to the deep ocean, which is questionable; hence, the results obtained here should be viewed as an exploration of the maximal potential effect of a productivity feedback.

5. Conclusions

[36] We have modified the Harvardton-Bear 3-box model for the oceanic carbonate system to predict the evolution of compensation dynamics under the IS92a loading scenario for atmospheric CO_2 in Figure 2. The model produces an atmospheric CO_2 history, anthropogenic fluxes to the ocean in the 1990–1999 period, and dissolution rates that are consistent with those from more sophisticated models; it also predicts pH and saturation state changes that are again quantitatively consistent with forecasts from coupled GCM-biogeochemical models. We have found that the modified Harvardton-Bear predicts that the saturation horizon will reach the top of the deep water (~0.25 km) within 500 years, even with dissolution of previously deposited carbonate. In other words, carbonate compensation acts too slowly to prevent a "runaway" undersaturation of the deep ocean. The carbonate compensation depth will rise, but reach an "apex" at ~1 km depth, before beginning to deepen again. The snowline will move up some 1150 m over this timeframe.

[37] If one adopts the additional assumption that the calcite compensation depth equals the saturation depth, then this creates a deep ocean with significantly weaker compensation dynamics. Adding a calcite production feedback in the low-latitude box causes a drastic narrowing in the difference between saturation and compensation horizons. The extent of calcification feedback in the real oceans thus needs to be firmly established. Adding an organic matter productivity feedback creates modest changes to benthic carbonate dynamics, but significantly affects gas exchange rates.

[38] All our predictions are possible because of better functional representations of dissolution and other related processes. While our modeling may at first appear to be more complicated with this approach, in fact the need for a diagenetic model has been completely eliminated, which constitutes a significant simplification in terms of both model formulation and solution.

[39] The modified Harvardton-Bear box model provides a means to explain to the broader scientific community the workings and the evolution of CO_2 in the oceans without inundating the reader with the physical complexity of the real oceans, a point argued by *Ridgwell* [2005]. The results reported here should be of utility to scientists attempting to predict the ocean's role in neutralizing the buildup of anthropogenic CO_2 in the atmosphere, to paleoceanographers attempting to model the movement of the carbonate compensation depth under past changes in atmospheric CO_2, and to geoengineers in their investigations of the potential for deep-sea sequestration of anthropogenic CO_2.

[40] **Acknowledgments.** This research was funded by the Natural Sciences and Engineering Research Council of Canada, the Netherlands Organization for Scientific Research, and the EU (European Project on Ocean Acidification (EPOCA)). We thank Bob Berner, Ken Caldeira, Robin Keir, Fred Mackenzie, Robert Moore, Greg Raviza, Helmut Thomas, and Richard Zeebe for critical comments on earlier versions of our manu-

script and two anonymous reviewers for constructive feedback on the current paper. The senior author also thanks Kathleen Ruttenberg for arranging a sabbatical visit to the University of Hawaii. This is publication 4870 of the Netherlands Institute of Ecology (NIOO-KNAW).

References

Amante, C., and B. W. Eakins (2009), ETOPO1 1 Arc-minute global relief model: Procedures, data sources and analysis, *NOAA Tech. Memo. NESDIS NGDC-24*. (Available at http://www.ngdc.noaa.gov/mgg/global/global.html)

Archer, D. E. (2005), Fate of fossil-fuel CO_2 in geologic time, *J. Geophys. Res.*, *110*, C09S05, doi:10.1029/2004JC002625.

Archer, D. E., and E. Maier-Reimer (1994), Effect of deep-sea sedimentary calcite preservation on atmospheric CO_2 concentration, *Nature*, *367*, 260–263, doi:10.1038/367260a0.

Archer, D. E., H. Kheshgi, and E. Maier-Reimer (1998), Dynamics of fossil fuel CO_2 neutralization by marine $CaCO_3$, *Global Biogeochem. Cycles*, *12*, 259–276, doi:10.1029/98GB00744.

Archer, D. E., G. Eshel, A. Winguth, W. Broecker, R. Pierrehumbert, M. Tobis, and R. Jacob (2000), Atmospheric pCO_2 sensitivity to the biological pump in the ocean, *Global Biogeochem. Cycles*, *14*, 1219–1230, doi:10.1029/1999GB001216.

Archer, D., et al. (2009), Atmospheric lifetime of fossil fuel carbon dioxide, *Annu. Rev. Earth Planet. Sci.*, *37*, 117–134, doi:10.1146/annurev.earth.031208.100206.

Berner, R. A., and Z. Kothavala (2001), GEOCARB III: A revised model of atmospheric CO_2 over Phanerozoic time, *Am. J. Sci.*, *301*, 182–204, doi:10.2475/ajs.301.2.182.

Boudreau, B. P. (2001), Solute transport above the sediment-water interface, in *The Benthic Boundary Layer: Transport Processes and Biogeochemistry*, edited by B. P. Boudreau and B. B. Jørgensen, pp. 104–126, Oxford Univ. Press, Oxford, U. K.

Boudreau, B. P., J. J. Middelburg, and F. J. R. Meysman (2010), Carbonate compensation dynamics, *Geophys. Res. Lett.*, *37*, L03603, doi:10.1029/2009GL041847.

Broecker, W. S. (2008), A need to improve reconstructions of the fluctuations in the calcite compensation depth over the course of the Cenozoic, *Paleoceanography*, *23*, PA1204, doi:10.1029/2007PA001456.

Broecker, W. S. (2009), Wally's quest to understand the ocean's $CaCO_3$ cycle, *Annu. Rev. Mar. Sci.*, *1*, 1–18, doi:10.1146/annurev.marine.010908.163936.

Broecker, W. S., and T.-H. Peng (1982), *Tracers in the Sea*, 690 pp., LDGO Press, Palisades, New York.

Broecker, W. S., and T.-H. Peng (1986), Glacial to interglacial changes in the operation of the global carbon cycle, *Radiocarbon*, *28*(2A), 309–327.

Broecker, W. S., J. Lynch-Stieglitz, D. Archer, M. Hofmann, E. Maier-Reimer, O. Marchal, T. Stocker, and N. Gruber (1999), How strong is the Harvardton-Bear constraint?, *Global Biogeochem. Cycles*, *13*, 817–820, doi:10.1029/1999GB900050.

Caldeira, K., and M. E. Wickett (2003), Anthropogenic carbon and ocean pH, *Nature*, *425*, 365, doi:10.1038/425365a.

Gehlen, M. R. Gangstø, B. Schneider, L. Bopp, O. Aumont, and C. Ethe (2007), The fate of pelagic $CaCO_3$ production in a high CO_2 ocean: Model study, *Biogeosciences*, *4*, 505–519, doi:10.5194/bg-4-505-2007.

Gruber, N., et al. (2009), Oceanic sources, sinks, and transport of atmospheric CO_2, *Global Biogeochem. Cycles*, *23*, GB1005, doi:10.1029/2008GB003349.

Keir, R. S. (1988), On the late Pleistocene ocean geochemistry and circulation, *Paleoceanography*, *3*(4), 413–445, doi:10.1029/PA003i004p00413.

Key, R. M., A. Kozyr, C. L. Sabine, K. Lee, R. Wanninkof, J. L. Bullister, R. A. Feely, F. J. Millero, C. Mordy, and T.-H. Peng (2004), A global ocean carbon climatology: Results from Global Data Analysis Project (GLODAP), *Global Biogeochem. Cycles*, *18*, GB4031, doi:10.1029/2004GB002247.

Khatiwala, S., F. Primeau, and T. Hall (2010), Reconstruction of the history of anthropogenic CO_2 concentrations in the ocean, *Nature*, *462*, 346–349, doi:10.1038/nature08526.

Knox, F., and M. B. McElroy (1984), Changes in atmospheric CO_2: Influence of the marine biota at high latitude, *J. Geophys. Res.*, *89*(D3), 4629–4637, doi:10.1029/JD089iD03p04629.

Lane, E., S. Peacock, and J. M. Restrepo (2006), A dynamic-flow carbon-cycle box model and high-latitude sensitivity, *Tellus, Ser. B*, *58*, 257–278.

Lenton, T. M., and C. Britton (2006), Enhanced carbonate and silicate weathering accelerates recovery from fossil fuel CO_2 perturbations, *Global Biogeochem. Cycles*, *20*, GB3009, doi:10.1029/2005GB002678.

Merico, A., T. Tyrell, and P. A. Wilson (2008), Eocene/Ologocene ocean de-acidification linked to Antarctic glaciation by sea-level fall, *Nature*, *452*, 979–982, doi:10.1038/nature06853.

Millero, F. J., T. B. Graham, F. Huang, H. Bustos-Serrano, and D. Pierrot (2006), Dissociation constants of carbonic acid in seawater as a function of salinity and temperature, *Mar. Chem.*, *100*, 80–94, doi:10.1016/j.marchem.2005.12.001.

Munhoven, G. (2007), Glacial-interglacial rain ratio changes: Implications for atmospheric CO_2 and ocean-sediment interaction, *Deep Sea Res, Part II*, *54*, 722–746, doi:10.1016/j.dsr2.2007.01.008.

Oxburgh, R. (1998), The Holocene preservation history of equatorial Pacific sediments, *Paleoceanography*, *13*, 50–62, doi:10.1029/97PA02607.

Ridgwell, A. (2005), A mid Mesozoic revolution in the regulation of ocean chemistry, *Mar. Geol.*, *217*, 339–357, doi:10.1016/j.margeo.2004.10.036.

Ridgwell, A., and J. C. Hargreaves (2007), Regulation of atmospheric CO_2 by deep-sea sediments in an Earth system model, *Global Biogeochem. Cycles*, *21*, GB2008, doi:10.1029/2006GB002764.

Ridgwell, A., and D. N. Schmidt (2010), Past constrains on the vulnerability of marine calcifiers to massive carbon dioxide release, *Nat. Geosci.*, *3*, 196–200, doi:10.1038/ngeo755.

Riebesell, U., et al. (2007), Enhanced biological carbon consumption in a high CO_2 ocean, *Nature*, *450*, 545–548, doi:10.1038/nature06267.

Roberts, C. D., and A. K. Tripati (2009), Modeled reconstructions of the oceanic carbonate system for different histories of atmospheric carbon dioxide during the last 20 Ma, *Global Biogeochem. Cycles*, *23*, GB1011, doi:10.1029/2008GB003310.

Sarmiento, J. J., and N. Gruber (2006), *Ocean Biogeochemical Dynamics*, 503 pp., Princeton Univ. Press, Princeton, N. J.

Sarmiento, J. L., and J. R. Toggweiler (1984), A new model for the role of the oceans in determining atmospheric pCO_2, *Nature*, *308*, 621–624, doi:10.1038/308621a0.

Siegenthaler, U., and T. Wenk (1984), Rapid atmospheric CO_2 variations and ocean circulation, *Nature*, *308*, 624–626, doi:10.1038/308624a0.

Stephens, B. B., and R. F. Keeling (2000), The influence of Antarctic sea ice on glacial-interglacial CO_2 variations, *Nature*, *404*, 171–174, doi:10.1038/35004556.

Toggweiler, J. R., S. Carson Gnanadesikan, R. Murmane, and J. L. Sarmiento (2003), Representation of the carbon cycle in box models and GCMs: 1. Solubility pump, *Global Biogeochem. Cycles*, *17*(1), 1026, doi:10.1029/2001GB001401.

Wigley, T. M. L., R. Richels, and J. A. Edmonds (1996), Economic and environmental choices in the stabilization of atmospheric CO_2 concentrations, *Nature*, *379*, 240–243, doi:10.1038/379240a0.

Zeebe, R. E., and P. A. Westbroek (2003), A simple model for the $CaCO_3$ saturation state of the ocean: The "Strangelove," the "Neritan," and the "Cretan" Ocean, *Geochem. Geophys. Geosyst.*, *4*(12), 1104, doi:10.1029/2003GC000538.

Zeebe, R. E., J. C. Zachos, and G. R. Dickens (2009), Carbon dioxide forcing alone insufficient to explain Paleocene-Eocene Thermal Maximum warming, *Nat. Geosci.*, *2*, 576–580, doi:10.1038/ngeo578.

B. P. Boudreau, Department of Oceanography, Dalhousie University, Halifax, NS B3H4J1 Canada. (bernie.boudreau@dal.ca)

A. F. Hofmann, Monterey Bay Aquarium Research Institute, Moss Landing, CA 95039, USA. (ahofmann@mbari.org)

F. J. R. Meysman, Netherlands Institute of Ecology, Yerseke, Netherlands. (f.meysman@nioo.knaw.nl)

J. J. Middelburg, Geochemistry, Faculty of Geosciences, University of Utrecht, Utrecht, Netherlands. (j.middelburg@geo.uu.nl)